Simulation numérique pour la caractérisation du cerveau par essai d'aspiration : Influence de l'anisotropie

Wael Alliliche, Christine Renaud, Jean-Michel Cros, Zhi-Qiang Feng

Numerical Simulation for Brain Characterization through Aspiration Test : Influence of Anisotropy.

W. ALLILICHE[a], C. RENAUD[a], J.M. CROS[a] and Z.Q. FENG[a]

a. Universite Paris-Saclay, Univ Evry, LMEE, 91020, Evry, France
wael.alliliche@univ-evry.fr

Abstract :

It has been demonstrated in the literature that the brain exhibits hyperelastic and anisotropic characteristics. We propose to model the behavior of the brain using the "HGO-Yeoh" law, which is both hyperelastic and anisotropic. This law is implemented in the Finite Element Research (FER) code, which already includes several developments, such as contact treatment using the bi-potential method. This allows us to simulate a suction test, showing that the behavior of brain tissue change depending on anisotropy. A sensitivity analysis followed by an inverse identification procedure based on experimental suction test data is also addressed in this study.

Keywords : Biomechanics, Brain, Hyperelastic, Constitutive law, Finite Elements, inverse identification.

1 Introduction

Most organs that make up the human body are soft tissues, such as the arteries, heart, intestines, skin and brain. The ability to predict human brain behaviour and evaluate changes in the mechanical properties of the tissue would inform engineering design. It would prove valuable in various disciplines : medical research and cancer diagnose. A soft tissue behaves as a hyperelastic material. It is almost incompressible because it is mainly made of water [20]. The brain is often likened to an isotropic hyperelastic material in classical models. However, its internal organization gives it anisotropic properties [8]. Many constitutive laws are used to model soft tissues in the literature. Some represent isotropic behaviour, such as neo-Hookean [13], Mooney-Rivlin [17], 8-chain [3], Yeoh [21], and Gent [9] models. The main difference between them is the trend of the stress-strain curve. Other laws describe both the isotropic and anisotropic behaviours, for example, the HGO [12], HGO-Yeoh [2] and the polyconvex [4] models.

This study aims to characterize the mechanical behavior of brain tissue using a numerical approach integrating the anisotropic hyperelastic behavior law HGO-Yeoh [2]. The adopted approach relies on using this law in a finite element (FEM) code [7], capable of efficiently handling complex contact-related issues through a method based on the bi-potential [6].

The suction test from the literature [18] was modeled through an axisymmetric problem to reduce computation times while maintaining satisfactory precision. This approach involves modeling the brain as a thick hyperelastic circular slice and the succion tube as a rigid hollow cylinder. By imposing a progressive negative pressure in increments, the vertical displacements of the tissue were simulated. The

parameters of the anisotropic hyperelastic behavior law were identified using an optimization procedure based on a genetic algorithm.

Although the axisymmetric modeling is relevant for an initial approach, it does not allow visualization of the effects of anisotropy during the suction test. This limitation led us to perform a 3D simulation, using the same previously identified parameters. Indeed, the 3D simulations highlighted the impact of anisotropy, particularly on horizontal displacements, which vary depending on the fiber orientation, while vertical displacements remain largely unaffected.

2 Brain's anisotropic hyperelastic constitutive law

2.1 used invariants

For soft tissue in bio-mechanics, the materials are nonlinear, hyperelastic, and almost incompressible. To take into account the anisotropic of the material, a single direction (**a**) of fibres is chosen. The model assumes that the mean direction of collagen fibres remains aligned with the plane. Indeed, histological examination of the skin [14] indicates that the majority of collagen fibres in the dermis are parallel to the epidermis. The displacement between fibre and matrix plays a negligible role in the elastic behaviour of the skin, since we consider only the main direction of the fibres network. The results obtained from identification in section [2], indicate that the fact of neglecting the displacement between fibre and matrix has no influence. The fibres orientation components are :

$$\mathbf{a} = \{\cos(\alpha), 0, \sin(\alpha)\}, \tag{1}$$

where α is the angle between the collagen fibres and the longitudinal axis of the skin $\vec{x}$ (Fig. 1); This angle is referred to as the local reference frame of elements $(\vec{x},\vec{y},\vec{z})_{\text{local}}$. **M** is the orientation matrix of the fibres. α is the angle between the collagen fibres and the longitudinal axis of the skin $\vec{x}$ (Fig. 1). We

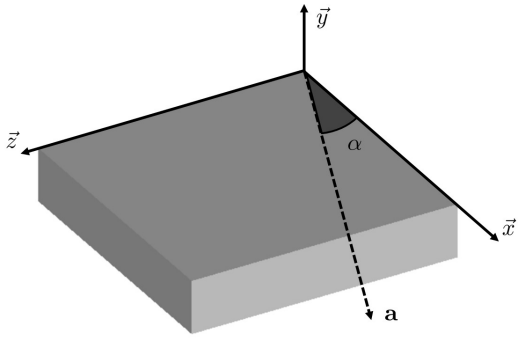

FIGURE 1 – Direction of the fibres $\vec{a}$ according to the angle α

note **M** as the orientation matrix of the fibres.

$$\mathbf{M} = (\mathbf{a} \otimes \mathbf{a}). \tag{2}$$

The transformation tensor $\mathbf{F}$, the Cauchy-Green strain $\mathbf{C}$ and the Green-Lagrange strain tensor $\mathbf{E}$ are defined as :

$$\mathbf{F} = \mathbf{I} + \frac{\partial \mathbf{u}}{\partial \mathbf{X}}, \tag{3}$$

$$\mathbf{C} = \mathbf{F}^T \mathbf{F}, \tag{4}$$

$$\mathbf{E} = \frac{1}{2}(\mathbf{C} - \mathbf{I}), \tag{5}$$

where $\mathbf{u}$ is the displacement vector and $\mathbf{I}$ is the identity matrix. Invariants I_1, I_3, I_4 and J are defined by :

$$I_1 = \mathrm{Tr}(\mathbf{C}), \tag{6}$$

$$I_3 = \det(\mathbf{C}), \tag{7}$$

$$I_4 = \mathrm{Tr}(\mathbf{C}\,\mathbf{M}), \tag{8}$$

$$J = \det(\mathbf{F}) = I_3^{\frac{1}{2}}. \tag{9}$$

J represents compression constraint and for isochoric deformation $J \approx 1$ [15]. Isochoric invariants of I_1 and I_4 are used in our model to consider compression variation by introducing I_3 :

$$\bar{I}_1 = I_1\, I_3^{-\frac{1}{3}}, \tag{10}$$

$$\bar{I}_4 = I_4\, I_3^{-\frac{1}{3}}. \tag{11}$$

2.2 HGO-Yeoh model

The anisotropy of the dermis is due to the collagen fibres, and the isotropy is due to the matrix. So, the behaviour law W is a sum of three deformation energies : isotropic W_{iso}, anisotropic W_{aniso} and volumetric W_{v}.

$$W = W_{\mathrm{iso}} + W_{\mathrm{aniso}} + W_{\mathrm{v}}. \tag{12}$$

To build the model, starting from the HGO model, whose isotropic part is the neo-Hookean model [$W_{iso} = a(I_1 - 3)$]. This part is replaced by the Yeoh model [$W_{iso} = a_i(I_1 - 3)^i$]. The HGO-Yeoh law contains two more parameters and a 3-order polynomial of I_1, which helps to have, as well, a good fitting as a better physical representation. This modification allows obtaining relevant results during the identification. The anisotropic term W_{aniso} [5] is composed of an exponential part that describes the effect of the fibres according to their orientation. Since the materials are nearly incompressible, the third term W_{v} describes compression behaviour. Each term of the equation (12) is given by :

$$W_{\mathrm{iso}}(\bar{I}_1) = \sum_{i=1}^{3} a_i(\bar{I}_1 - 3)^i, \tag{13}$$

$$W_{\mathrm{aniso}}(\bar{I}_4) = \frac{c_1}{2\,c_2}(e^{c_2\,(\bar{I}_4 - 1)^2} - 1), \tag{14}$$

$$W_{\mathrm{v}}(J) = \frac{1}{d}(J-1)^2. \tag{15}$$

The constants $a_1,\ a_2,\ a_3,\ c_1,\ c_2$ are the material parameters to be defined, d is an expansion parameter that is chosen very small $(d = 10^{-6})$ in incompressible cases, it models the hydrostatic pressure numerically.

In our constitutive model, the fibres only work in tensile. Therefore, there is no effect on the compression, so the part W_{aniso} is under these conditions :

$$\begin{cases} \text{if } I_4 < 1 \ W_{\text{aniso}}(\bar{I}_4) = 0 & \textit{Compression} \\ \text{if } I_4 \geq 1 \ W_{\text{aniso}}(\bar{I}_4) = \dfrac{c_1}{2\,c_2}(e^{c_2\,(\bar{I}_4-1)^2}-1) & \textit{Tensile} \end{cases} \tag{16}$$

2.3 Constraint calculation and implementation

In order to implement this model, the second Piola-Kirchhoff stress tensor $\mathbf{S}$ (17) is defined by derivating the potential W with respect to the strain tensor [16] :

$$\mathbf{S} = \frac{\partial W}{\partial \mathbf{E}} = 2\frac{\partial W}{\partial \mathbf{C}}. \tag{17}$$

Then the calculus by using the partial derivative of $\mathbf{S}$ (17) is developed :

$$\mathbf{S} = 2\frac{\partial W}{\partial \mathbf{C}} \tag{18}$$

$$= 2\left(\frac{\partial W}{\partial I_1}\frac{\partial I_1}{\partial \mathbf{C}} + \frac{\partial W}{\partial I_3}\frac{\partial I_3}{\partial \mathbf{C}} + \frac{\partial W}{\partial I_4}\frac{\partial I_4}{\partial \mathbf{C}} + \frac{\partial W}{\partial J}\frac{\partial J}{\partial \mathbf{C}}\right). \tag{19}$$

This formula of Piola-Kirchhoff constraints is developed by injecting the partial derivatives of W (13) as well as the derivative of the invariants (9) into $\mathbf{S}$ (17) :

$$\begin{aligned} \mathbf{S} =& 2\left(\frac{\partial W}{\partial I_1}\mathbf{I} + \frac{\partial W}{\partial I_3}\mathrm{Coef}(\mathbf{C})\right. \\ &\left. + \frac{\partial W}{\partial I_4}\mathbf{M} + \frac{\partial W}{\partial J}\,\frac{1}{2}\,J\,\mathbf{C}^{-T}\right). \end{aligned} \tag{20}$$

Then, the Cauchy stress tensor $\boldsymbol{\sigma}$ is deduced from $\mathbf{S}$ (17) and transformation tensor $\mathbf{F}$ (3) :

$$\boldsymbol{\sigma} = \frac{1}{J}\,\mathbf{F}\,\mathbf{S}\,\mathbf{F}^T. \tag{21}$$

3 Inverse identification of brain tissue parameters through optimization

In the context of inverse identification, optimization methods play a crucial role in enabling the precise estimation of parameters in a mathematical model from experimental data. These methods are used to adjust parameter values to improve the match between model predictions and real-world observations. In this section, we will discuss optimization methods in the inverse identification process, focusing on the use of MATLAB genetic algorithm. We will also examine the Pearson determination coefficient as the objective function to guide the optimization.

3.1 Succion expérimental test

The suction test involves applying a negative pressure perpendicular to the tissue for a few seconds using a suction tube, known as a depression chamber (figure 2). The hyperelastic material then forms a dome-like shape inside the tube. The objective is to measure the deflection, which corresponds to the height of this dome, as a function of pressure.

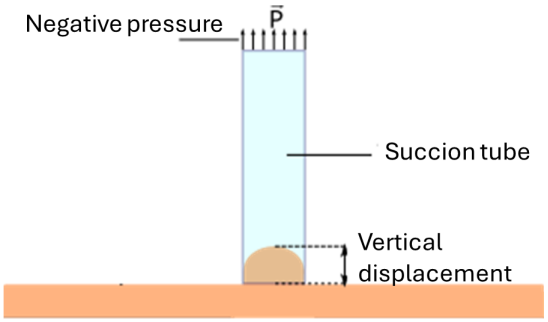

FIGURE 2 – Suction test

The dimensions of the chamber and the intensity of the depression are important factors in identifying the material parameters ; a larger radius allows for the identification of tissue at a greater depth. In our case, we obtained data from [18], which performs a suction test on the brain in vivo.

3.2 Numerical Modeling of the Suction Test on the Brain

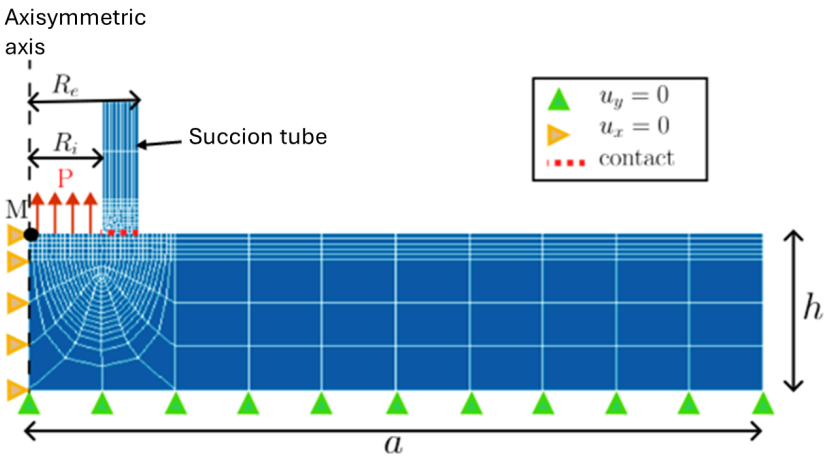

FIGURE 3 – Finite element model and boundary conditions for suction experiments $R_e = 7.5$ mm, $R_i = 5$ mm, $a = 100$ mm, $h = 25$ mm.

Due to the presence of contact, the suction model cannot be solved analytically. A finite element analysis was performed using the FER code, modeling the brain as a thick circular slice and the seccion tube as a rigid hollow cylinder. This problem was modeled as a 2D axisymmetric structure, allowing for time savings during identification and simulations. This required the integration of an axisymmetric element into the FER code.

To determine a precise mesh that does not influence the results during identification, we plotted (figure 4) the evolution of the maximum displacement of point M as a function of the number of finite elements. This convergence analysis aims to identify the minimum number of elements required to ensure accurate

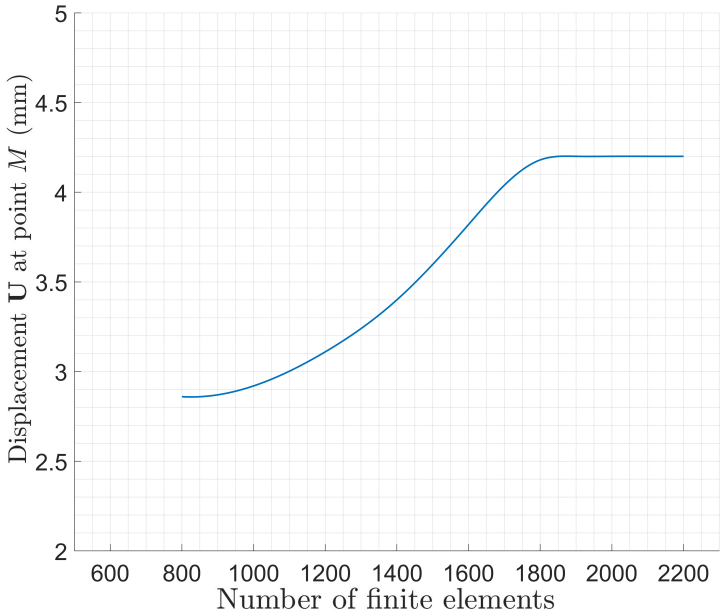

FIGURE 4 – Sensitivity of displacement of point M to the number of finite elements

results while optimizing computation time. To achieve this, the mesh was refined in sensitive areas, particularly in regions of contact, pressure application, and boundary conditions.

For a number of elements less than 800, the model does not converge, indicating that the mesh is insufficient to capture the mechanical response.

Between 800 and 1,800 elements, the displacement of M remains sensitive to mesh variations. Any change in the number of elements within this range results in significant changes in the results.

Beyond 1,800 elements, the results stabilize. The displacements become insensitive to the number of elements, showing that convergence is achieved. Further refinement of the mesh does not improve precision but significantly increases computation time. Based on these observations, 1,800 elements were chosen for optimal calculation. This mesh ensures reliable convergence while reducing computational cost.

The bi-potential method [7] is used to handle contact between the sucction tube and the sample interface. To model the absence of friction as indicated in [18] and ensure convergence, a null friction coefficient between the glass tube and the brain is applied, $\mu^{\text{brain}-\text{Glass}} = 0.0$. A fillet is added to the tube (figure 5), at the point of contact, to avoid a singularity point.

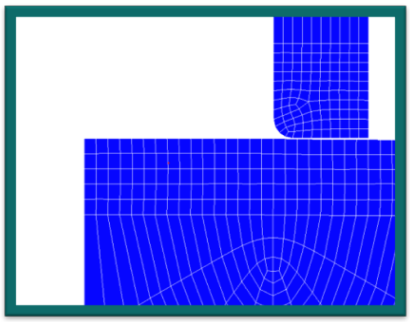

FIGURE 5 – Representation of finite element modeling with fillet

100 load increments are applied by imposing a negative pressure P of 25 mbar at each increment. We measure the vertical displacement of point M at each step. For the material behavior, we chose to use the HGO-Yeoh model [1]. For identification, we arbitrarily chose a fiber orientation angle of $\alpha = 45°$, as data regarding anisotropy were not provided.

Once the displacement of point M as a function of pressure progression is obtained, the displacement field is used during the identification presented in paragraph 3.6.

3.3 Sensitivity Analysis of the HGO-Yeoh Model in Succion

This analysis aims to evaluate the sensitivity and influence of various parameters of the HGO-Yeoh model on the mechanical response during the succion test. The results highlight the dominant and secondary parameters, providing a useful hierarchy for optimizing and simplifying the parameter identification process.

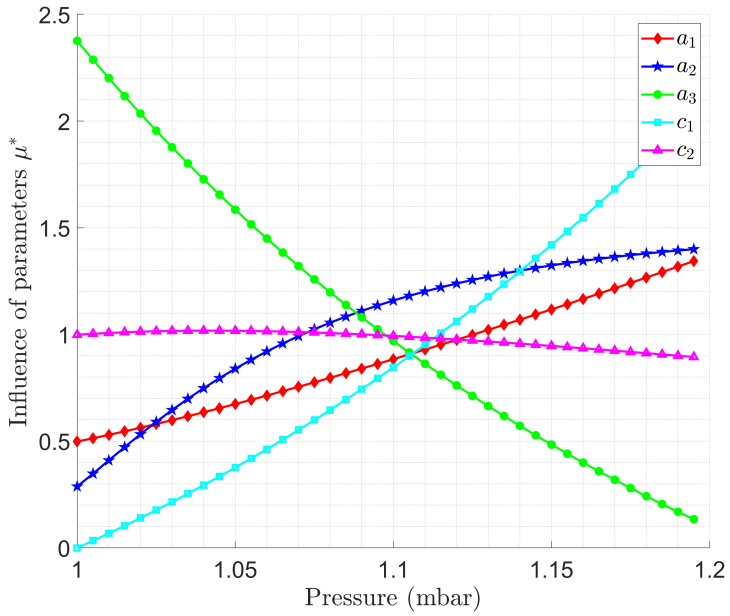

FIGURE 6 – Gradient : Influence of each parameter as a function of pressure evolution

Figure 6 illustrates the relative effect (μ^*) of the model parameters as a function of pressure during the aspiration test. The evolution of the curves reveals notable variations in the influence of different parameters as the pressure increases.

The parameters a_1 and a_2 follow similar trends with increasing influence as the pressure rises. Their contributions evolve differently : the influence of a_1 follows a linear trend, while that of a_2 is non-linear, converging to a constant gradient value, highlighting their important role in representing the mechanical response throughout the test.

The parameter a_3 stands out with an inverse behavior. It is dominant at the beginning of the test, with a high initial influence ($\mu^* \approx 2.5$), but its importance continuously decreases as the pressure increases. This progressive decline reflects that a_3 is essential for modeling initial behaviors under low pressures, but its role becomes secondary at higher pressures.

The parameter c_1 experiences a marked increase in influence with pressure, transitioning from a minor role at the start of the test to a dominant contribution at high pressure. In contrast, the parameter c_2

exhibits a different behavior, with its influence slightly decreasing throughout the test. This increasing behavior of c_1 underscores its importance in modeling at high pressures.

In conclusion, this analysis identifies distinct groups of parameters. The parameters a_1, a_2, and c_1 are the most influential at high pressure, while a_3 plays a significant role at low pressures. c_2 has a nearly constant and slightly decreasing influence throughout the test. These observations guide the identification process by prioritizing dominant parameters in the pressure ranges where they have the most impact, while simplifying the analysis of less influential parameters.

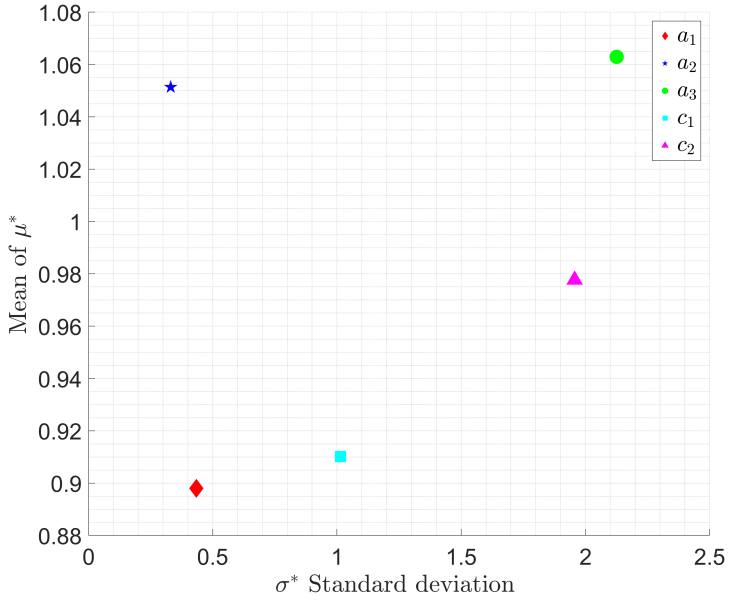

FIGURE 7 – Morris Index : Influence of each parameter on the aspiration model

Figure 7 highlights the global sensitivity of the parameters (μ^*) and their influence on non-linearity (σ^*).

The parameters a_1 and c_1 show low global sensitivity (μ^*) and limited influence on non-linearity (σ^*). These parameters play a relatively minor role in the overall mechanical response, with their contribution remaining essentially linear. Although their influence is low, it is still significant, as it exceeds 10% of the maximum value observed here for a_3. This underscores that, even though they do not dominate the model's response, a_1 and c_1 contribute to overall precision and should not be neglected.

In contrast, a_2 and c_2 exhibit more contrasting behaviors. a_2 shows strong global sensitivity and a low contribution to non-linearity, giving it intermediate importance in the model. c_2, while moderately sensitive, plays a more pronounced role in non-linear regimes.

The parameter a_3 stands out from the others. With high sensitivity and a strong influence on non-linearity, it plays a key role in the model. Its dual influence on the global response and non-linear behaviors makes it a central parameter to consider for modeling and optimization.

Thus, this analysis shows that some parameters, like a_1 and c_1, have a minor but non-negligible contribution, while others, like a_3, are essential for capturing both the global sensitivity and the non-linear contribution of the model. This hierarchizes their importance for effective analysis and identification.

3.4 Objective Function : Pearson's Coefficient of Determination

Pearson's coefficient of determination, denoted as R^2, is a measure of the quality of a linear regression prediction [19]. It is defined by :

$$R^2 = 1 - \frac{\sum_{i=1}^{n}(y_i - y^{\text{model}})^2}{\sum_{i=1}^{n}(y_i - y^{\text{mean}})^2}, \tag{22}$$

where n represents the number of measurements, y_i is the measured value, y^{mean} is the mean of the measurements, and y^{model} is the value predicted by the model. It can also be written as :

$$R^2 = 1 - \frac{S_{\text{res}}}{S_{\text{tot}}}, \tag{23}$$

with S_{tot} being the total sum of squares and S_{res} the residual sum of squares. The closer the coefficient value is to 1, the higher the predictive power of the model. The algorithm aims to minimize $\frac{S_{\text{res}}}{S_{\text{tot}}}$. This function, widely used in statistics, is suitable for comparing models with experiments. This objective function allows for convergence to a more precise result by avoiding local minima.

3.5 Optimization Methods : Genetic Algorithm

The genetic algorithm is designed based on the principles of Darwinian natural selection, characterized by sexual reproduction and the predominance of the survival of the fittest individuals [10]. According to Darwinian theory, the concept of "survival of the fittest" implies that entities with superior adaptability and task execution capabilities in their environment, commonly referred to as the "fittest," dominate and reproduce more frequently. Conversely, less fit entities tend to survive and reproduce at a lower rate.

John Holland [11] developed a mathematical simulation of evolution that emphasizes natural selection and the principle of survival. In his model, he considers the crossover between genes to find the most performing individuals. Genetic algorithms view mutation as a secondary tool. Thus, the fundamental steps of a genetic algorithm are : selection based on performance, crossover, and mutation as a complementary tool. To configure a genetic optimization algorithm, we must determine the population size, the number of generations, a criterion, and a mutation rate. These parameters are determined based on the number of parameters to be calculated and the complexity of the problem.

In a genetic algorithm, after creating an initial random population, the process begins by evaluating this population to determine the genetic characteristics and performance of each individual. These characterized individuals then replace their predecessors to form a new generation of parents, carrying genes to be passed on. If among these parents, an individual meets the performance criteria and satisfies the pre-established stopping conditions, it is selected as the solution to the problem, ending the iteration.

If no individual meets these criteria, the process continues. Parents are chosen for reproduction, and their offspring are generated primarily through the crossover of parameters from two individuals. This operation is completed by the automatic replication of the parents' genes with random genetic mutations, according to the predefined mutation rate. This cycle of evaluation, selection, crossover, and mutation repeats until an individual satisfies the stopping criteria, thus providing an optimized solution to the problem.

3.6 Inverse identification of the HGO-Yeoh model

The identification algorithm implemented in MATLAB follows the steps described in the algorithm (figure 8). This algorithm aims to optimize the parameters specified in the input file by iteratively adjusting them and evaluating the objective function. In doing so, it seeks to discover the optimal set of parameters that minimizes or maximizes the function, depending on the problem statement.

For this study, we chose to use the anisotropic hyperelastic HGO-Yeoh law. A simpler law, such as the neo-Hookean, Mooney-Rivlin, or Yeoh laws, would have sufficed for identifying experimental data. However, our goal is to explore the influence of anisotropy on mechanical behavior in an equivalent 3D model.

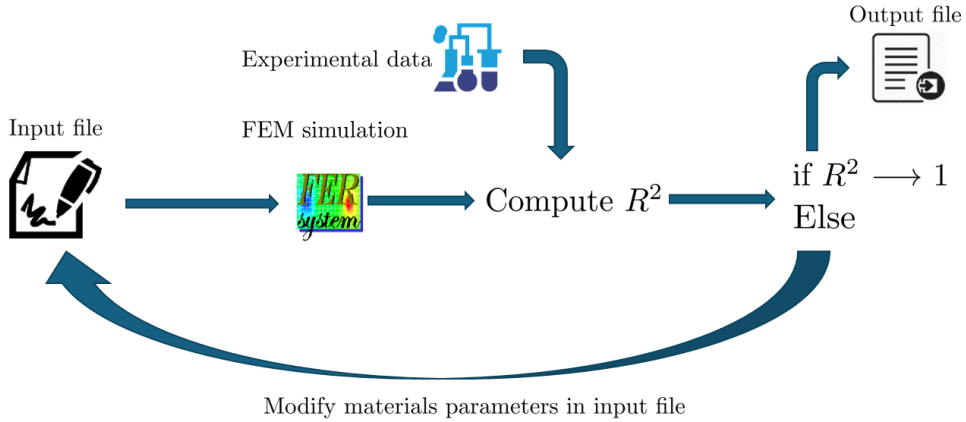

FIGURE 8 – Parameter identification process

In our approach, we configured the genetic algorithm with 25 generations and a population size of 100 individuals, or 20 per parameter. To compensate for simulations where the Newton-Raphson algorithm does not converge, we used twice as many individuals as recommended. We then set a default mutation coefficient of 30%, which was crucial in the final generations for refining the results. By using a larger population size, the algorithm can explore a broader range of potential solutions in each generation. This increased diversity helps mitigate the risk of prematurely converging to a local minimum.

The algorithm we used follows an iterative process encompassing several key steps, beginning with initialization where data is collected, and the initial model parameters are defined. Then, finite element processing (FEM) is applied, using the provided parameters to perform a detailed analysis of the model and calculate the displacement vector as a function of the applied pressure. This process includes comparing the calculated displacements with those from the experiment [18], followed by calculating the coefficient of determination (R^2) to evaluate the correspondence between the modeled and experimental results. The convergence of the algorithm is determined by achieving an R^2 close to 1 with an error margin of 10^{-3}. If this convergence condition is met, the final parameters are saved to an output file. Otherwise, the algorithm can be reiterated to further refine the results, ensuring continuous optimization until the convergence criteria are met. The identification time was much longer than when using an analytical equation-based identification. It took us 8 hours and 35 minutes to obtain the identified parameters. The parameters obtained after optimization are given in table 1.

To visualize the optimization results, we plotted the displacement $\mathbf{U}_y^{\text{num}}$ obtained from numerical calculations and the displacement $\mathbf{U}_y^{\text{exp}}$ obtained from experimental data. Both displacements are plotted as a function of the progressively applied pressure on the brain.

Finally, to deepen our comparison, we calculated the relative error between the numerical results and the experimental data (figure 10). The maximum error for the HGO-Yeoh model reaches 2.35%, while the average is 0.58%.

The results obtained in this study demonstrate our ability to predict the behavior of soft tissues using the finite element method, employing the contact method based on the bi-potential. By integrating our finite

TABLE 1 – Identified parameters for the HGO-Yeoh model for a succion test on the brain

Parameters	HGO-Yeoh
a_1 (MPa)	5.122 e^{-3}
a_2 (MPa)	2.324 e^{-3}
a_3 (MPa)	3.290 e^{-3}
c_1 (MPa)	1.391 e^{-3}
c_2	- 3.43

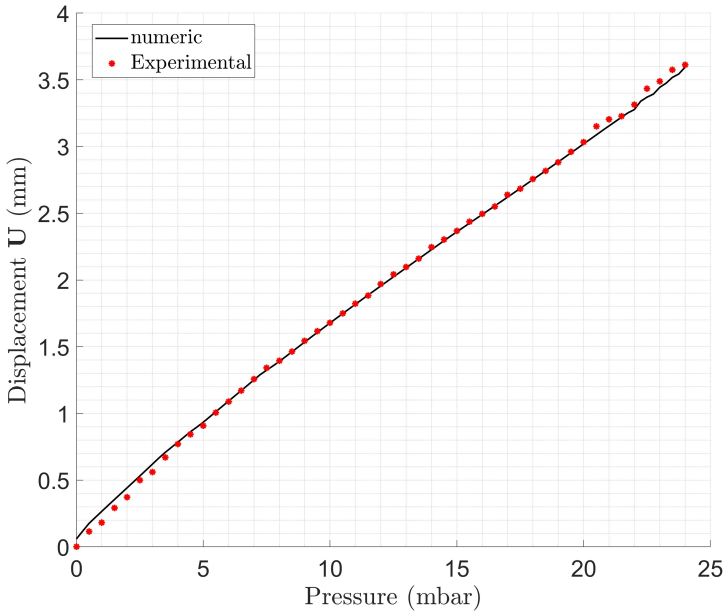

FIGURE 9 – Comparison of experimental succion results on the brain with predictions from the HGO-Yeoh hyperelastic laws

element calculation code with an optimization strategy that employs a genetic algorithm, we successfully characterized brain tissue during a complex test. The succion test leads to contact between the succion tube and the soft tissue, a phenomenon that is difficult to model analytically. This method can also be applied to other types of tests, such as indentation and twist tests, which are used for the in vivo characterization of soft tissues.

4 Results : Simulation of sucction test on the brain

We apply the HGO-Yeoh behavior law, whose parameters were identified in the previous chapter (table 1). The initial results are obtained through a simulation using an axisymmetric model described in section 3.2.

Subsequently, we expand our analysis using a 3D model of the brain test that accounts for anisotropy. This allows us to better visualize the effect of anisotropy on the tissue.

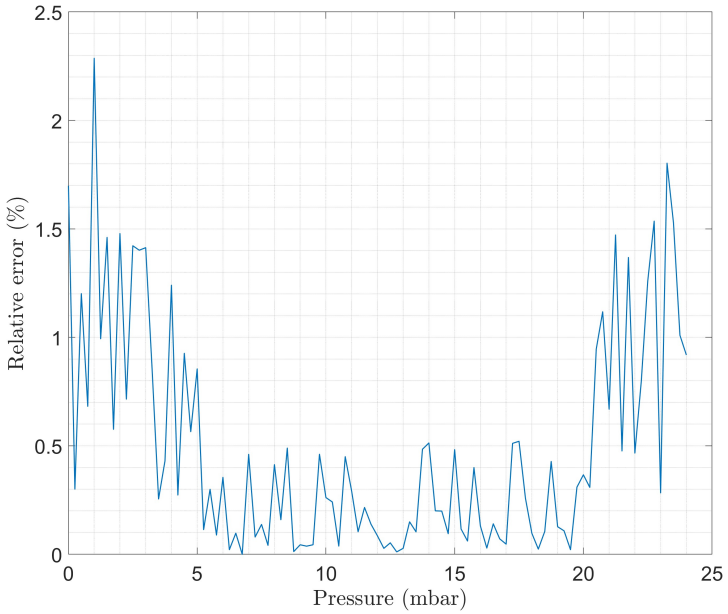

FIGURE 10 – Relative error between experimental succion data on the brain and numerical results

4.1 Description of the 3D Aspiration Test Modeling

In the 3D model of the succion test, we represent $\frac{1}{4}$ of the structure (figure 11). We modeled the brain as a parallelepiped with dimensions 100 mm x 50 mm x 100 mm in a global coordinate system $(\vec{x},\vec{y},\vec{z})_{\text{global}}$. A quarter cylinder with an inner radius of 5 mm and an outer radius of 7.5 mm is used to model the succion tube. We obtain a mesh with 4,807 nodes and 3,628 eight-node hexahedral elements. We will use the parameters of the HGO-Yeoh law obtained during the identification in section 3.6. To limit friction as indicated in [18], we use a friction coefficient between the brain and the glass succion tube of $\mu^{\text{cerv}-\text{verre}} = 0.01$.

Next, we apply a pressure of 0.24 mbar in 100 increments to gradually reach a pressure of 24 mbar.

We fix 2 key points M, W (figure 11) to explore the results in the following section.

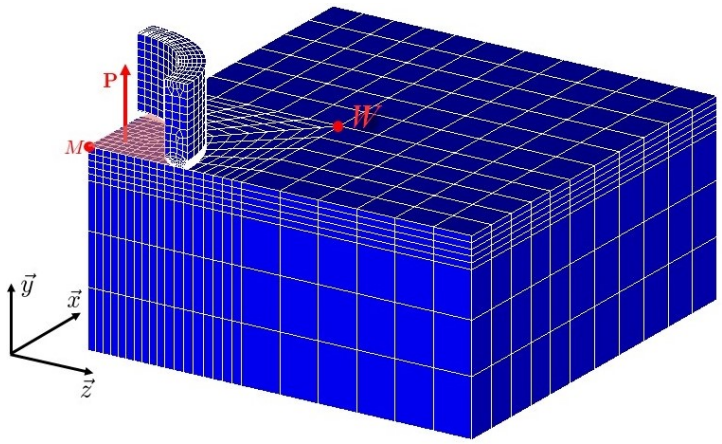

FIGURE 11 – 3D finite element model of the succion test

4.2 Analysis of Results and Discussion

Figure 12 shows the numerical simulation results of the axisymmetric succion test, with a zoom on the most interesting part, as the rest of the structure does not undergo significant deformations.

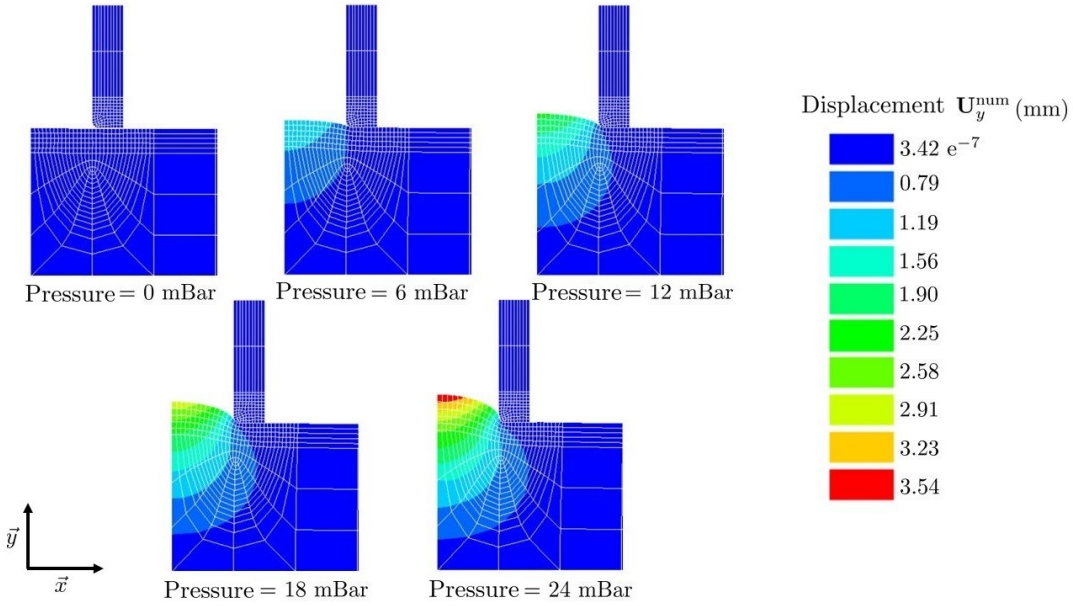

FIGURE 12 – Visualization of displacements U_y^{num} as a function of pressure evolution in an axisymmetric model

In the figure, we see five states of the sample structure, indicating the deformations under different pressures. The colors on the sample change from blue (minimal displacement) to red (maximal displacement), according to the scale on the right, which indicates the vertical displacement in millimeters. As the pressure increases, figure 12 shows the evolution of vertical displacements and the areas affected by these displacements.

These results do not show the effect of anisotropy, which is why we added a simulation with a 3D model to our study. We display in figure 13 the displacement U_y^{brain} as a function of different pressures. We notice that qualitatively, the 3D behavior is similar to that of the axisymmetric problem.

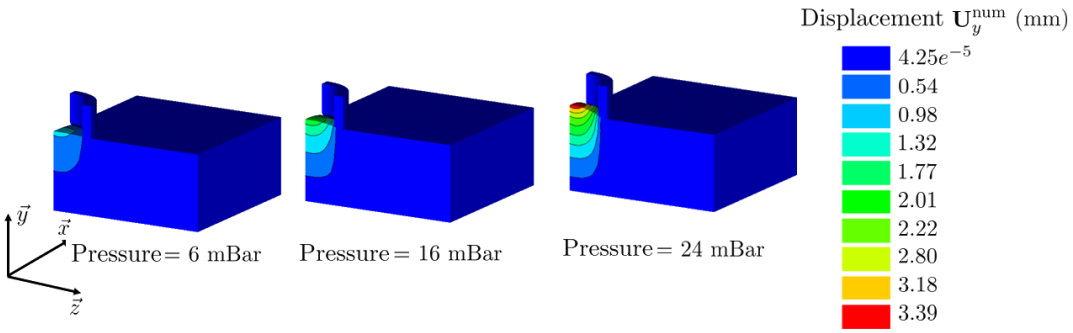

FIGURE 13 – Visualization of brain tissue displacements U_y^{num} as a function of pressure evolution in 3D

From a quantitative perspective, we compare the numerical results obtained via the axisymmetric simulation $U_y^{\text{brain}-\text{axi}}$ and those from the 3D model $U_y^{\text{brain}-\text{3D}}$ of the displacement as a function of pressure evolution at point M (figure 14).

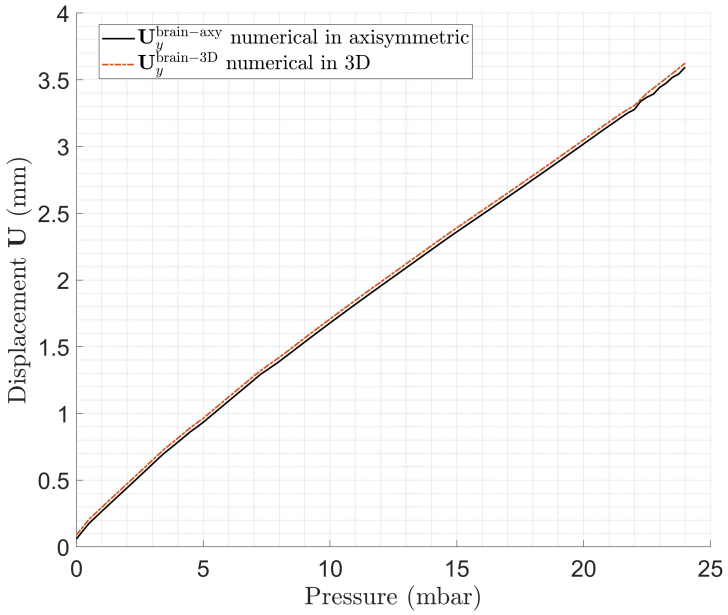

FIGURE 14 – Comparison between axisymmetric results $U_y^{\text{brain}-\text{axy}}$ and 3D results $U_y^{\text{brain}-\text{3D}}$

The results show similar trends with a maximum relative error of 1.5%. This can be primarily attributed to differences in modeling, such as the number of elements used or the number of contact points between the models. This acceptable result allows us to study the effect of anisotropy during the succion test.

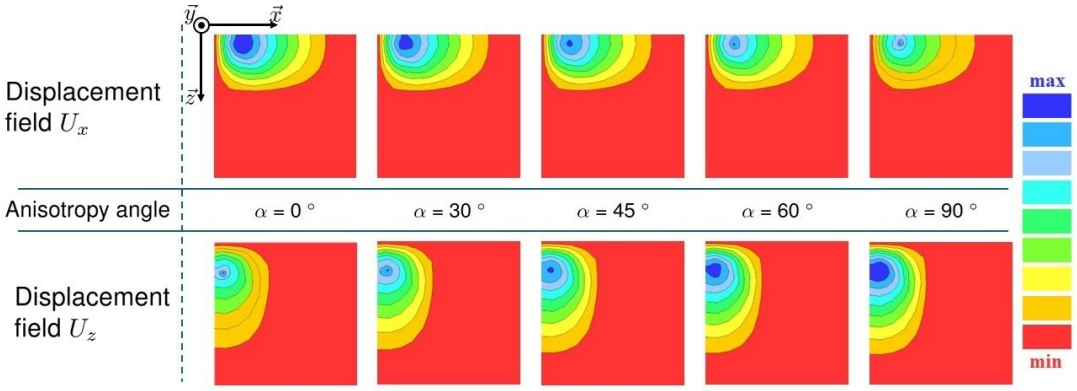

FIGURE 15 – Visualization of brain tissue displacements as a function of anisotropy variation

To study the effect of fiber orientation, we display in figure 15 the distribution of displacements U_x and U_z of the sample as a function of different angles α (1). The results allow us to qualitatively visualize the effect of anisotropy. Unlike the displacement U_y^{brain}, which does not vary with fiber orientation, the horizontal displacements U_x^{brain} and U_z^{brain} change with anisotropy. Indeed, the displacement $||U_x^{\text{brain}}||$ is minimal when $\alpha = 0°$. This displacement decreases in intensity to reach its maximum at $\alpha = 90°$. The displacement $||U_z^{\text{brain}}||$ exhibits the opposite behavior compared to $||U_x^{\text{brain}}||$.

To quantify this observation, we display in figure 16 the variation of U_x^{brain} and U_x^{brain} at point W as a function of the angles relative to anisotropy.

Our analysis indicates that the displacement in U_y^{brain} remains constant regardless of the material's anisotropy. However, we observe in figure (16) displacements in U_x^{brain} and U_z^{brain} that vary by up to 20%. These observations allow us to conclude that the succion test is primarily suited for characterizing

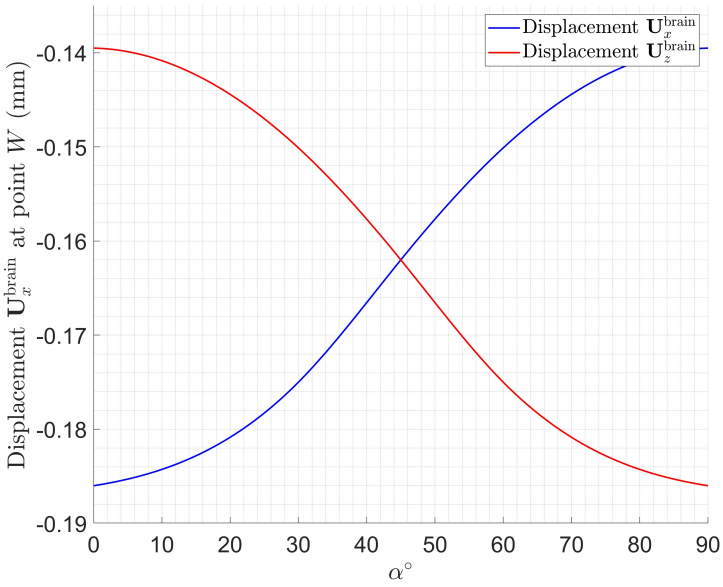

FIGURE 16 – Variation of displacements U_x^{brain} and U_z^{brain} at point W as a function of anisotropy

isotropic materials, as the element controlling the output, U_y^{brain}, of the identification function is not affected by the angle relative to anisotropy. However, even though we observe an effect of anisotropy on the other displacements (U_x^{brain} and U_z^{brain}), without additional experimental data, we cannot fully validate our model.

5 Conclusion

The study presented here focuses on characterizing the mechanical behavior of brain tissue using the anisotropic hyperelastic HGO-Yeoh model, integrated within a finite element framework. By employing a genetic algorithm for parameter identification and conducting sensitivity analyses, the research successfully simulated a succion test on brain tissue, demonstrating good agreement with experimental data. The 3D simulations highlighted the significant impact of anisotropy on horizontal displacements, revealing variations of up to 20% depending on fiber orientation. This work underscores the importance of considering anisotropy in brain tissue modeling and provides a robust methodological framework for future biomechanical studies. The integration of advanced numerical techniques, such as the bi-potential method for contact handling, ensured accurate and stable simulations, paving the way for applications in surgical planning and injury prevention. However, further validation with additional experimental data is necessary to fully understand the anisotropic behavior of brain tissue. Overall, this study contributes to the broader understanding of brain biomechanics and emphasizes the need for comprehensive modeling approaches to capture the complex mechanical responses of soft tissues.

Références

[1] W. ALLILICHE, C. RENAUD, J.-M. CROS et Z.-Q. FENG, "An anisotropic hyperelastic model for human skin : finite element modeling, identification of parameters, mechanical tests," *Computer Methods, Imaging and Visualization in Biomechanics and Biomedical Engineering II*, 2023.

[2] W. Alliliche, C. Renaud, J.-M. Cros et Z.-Q. Feng, "Numerical simulation of mechanical tests on a living skin using anisotropic hyperelastic law," *Journal of the Mechanical Behavior of Biomedical Materials*, t. 141, p. 105 755, 2023.

[3] E. M. Arruda et M. C. Boyce, "A three-dimensional constitutive model for the large stretch behavior of rubber elastic materials," *Journal of the Mechanics and Physics of Solids*, t. 41, n° 2, p. 389-412, 1993.

[4] R. Cai, L. Hu, F. Holweck, F. Peyraut et Z.-Q. Feng, "Convexity, polyconvexity and finite element implementation of a four-fiber anisotropic hyperelastic strain energy density—Application to the modeling of femoral, popliteal and tibial arteries," *Computer Methods in Applied Mechanics and Engineering*, t. 399, p. 115 294, 2022.

[5] G. Chagnon, G. Marckmann et E. Verron, "A Comparison of the Hart-Smith Model with Arruda-Boyce and Gent Formulations for Rubber Elasticity," *Rubber Chemistry and Technology*, t. 77, n° 4, p. 724-735, 2004.

[6] G. De Saxcé et Z.-Q. Feng, "New inequality and functional for contact with friction : the implicit standard material approach," *Mechanics of Structures and Machines*, t. 19, p. 301-325, 1991.

[7] G. De Saxcé et Z.-Q. Feng, "The bi-potential method : a constructive approach to design the complete contact law with friction and improved numerical algorithms," *Mathematical and Computer Modeling*, t. 28(4-8), p. 225-245, 1998.

[8] F. Eskandari, M. Shafieian, M. M. Aghdam et K. Laksari, "Tension Strain-Softening and compression Strain-Stiffening behavior of brain white matter," en, *Ann Biomed Eng*, t. 49, n° 1, p. 276-286, juin 2020.

[9] A. N. Gent, "A new constitutive relation for rubber," *Rubber Chemistry and Technology*, t. 69, n° 1, p. 59-61, 1996.

[10] N. Harb, "Identification inverse de paramètres biomécaniques en hyperélasticité anisotrope," thèse de doct., Université de Technologie de Belfort-Montbeliard, 2013.

[11] J. H. Holland, *Adaptation in Natural and Artificial Systems : An Introductory Analysis with Applications to Biology, Control, and Artificial Intelligence*. The MIT Press, 1992.

[12] G. A. Holzapfel, T. C. Gasser et R. W. Ogden, "A new constitutive framework for arterial wall mechanics and a comparative study of material models," *Journal of elasticity and the physical science of solids*, t. 61, p. 1-48, 2000.

[13] M. Mooney, "A theory of large elastic deformation," *Journal of Applied Physics*, t. 11, p. 582-592, 1940.

[14] A. Ní Annaidh et al., "Automated estimation of collagen fibre dispersion in the dermis and its contribution to the anisotropic behaviour of skin," *Annals of Biomedical Engineering*, t. 40, n° 8, p. 1666-1678, 2012.

[15] R. W. Ogden, *Non-linear elastic deformations*. Courier Corporation, 1997.

[16] F. Peyraut, C. Renaud, N. Labed et Z.-Q. Feng, "Modélisation de tissus biologiques en hyperélasticité anisotrope – étude théorique et approche éléments finis," *Comptes Rendus Mécanique*, t. 337, n° 2, p. 101-106, 2009.

[17] R. Rivlin, "Large elastic deformations of isotropic materials," *Philosophical Transcription of the Royal Society of London*, t. 240, p. 491-508, 1948.

[18] P. Schiavone, F. Chassat, T. Boudou, E. Promayon, F. Valdivia et Y. Payan, "In vivo measurement of human brain elasticity using a light aspiration device," *Med Image Anal*, t. 13, n° 4, p. 673-678, 2009.

[19] P. Schober, C. Boer et L. A. Schwarte, "Correlation coefficients : appropriate use and interpretation," *Anesthesia & Analgesia*, t. 126, n° 5, p. 1763-1768, 2018.

[20] F. Xu et T. Lu, *Introduction to Skin Biothermomechanics and Thermal Pain*. Springer Berlin Heidelberg, 2011.

[21] O. H. Yeoh, "Some forms of the strain energy function for rubber," *Rubber Chemistry and Technology*, t. 66, n° 5, p. 754-771, 1993.